University of Nebraska - Lincoln
DigitalCommons@University of Nebraska - Lincoln

Architecture Program: Faculty Scholarly and Creative Activity

Architecture Program

2022

From cropland to cropped field: A robust algorithm for national-scale mapping by fusing time series of Sentinel-1 and Sentinel-2

Bingwen Qiu

Duoduo Lin

Chongcheng Chen

Peng Yang

Zhenghong Tang

See next page for additional authors

Follow this and additional works at: https://digitalcommons.unl.edu/arch_facultyschol

 Part of the Urban, Community and Regional Planning Commons

This Article is brought to you for free and open access by the Architecture Program at DigitalCommons@University of Nebraska - Lincoln. It has been accepted for inclusion in Architecture Program: Faculty Scholarly and Creative Activity by an authorized administrator of DigitalCommons@University of Nebraska - Lincoln.

Authors

Bingwen Qiu, Duoduo Lin, Chongcheng Chen, Peng Yang, Zhenghong Tang, Zhenong Jin, Zhiyan Ye, Xiao Zhu, Mingjie Duan, Hangyu Huang, Zhiyuan Zhao, Weiming Xu, and Zuoqi Chen

International Journal of Applied Earth Observations and Geoinformation 113 (2022) 103006

Contents lists available at ScienceDirect

International Journal of Applied Earth Observations and Geoinformation

journal homepage: www.elsevier.com/locate/jag

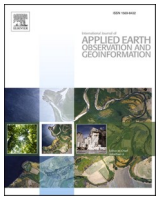

From cropland to cropped field: A robust algorithm for national-scale mapping by fusing time series of Sentinel-1 and Sentinel-2

Bingwen Qiu [a,*], Duoduo Lin [a], Chongcheng Chen [a], Peng Yang [b], Zhenghong Tang [c], Zhenong Jin [d], Zhiyan Ye [a], Xiaolin Zhu [e], Mingjie Duan [e], Hongyu Huang [a], Zhiyuan Zhao [a], Weiming Xu [a], Zuoqi Chen [a]

[a] Key Laboratory of Spatial Data Mining &Information Sharing of Ministry of Education, Academy of Digital China (Fujian), Fuzhou University, Fuzhou 350116, Fujian, China
[b] Key Laboratory of Agricultural Remote Sensing, Ministry of Agriculture and Rural Affairs, Beijing, China
[c] Community and Regional Planning Program, University of Nebraska-Lincoln, Lincoln 68558, NB, United States
[d] Department of Bioproducts and Biosystems Engineering, University of Minnesota, St. Paul 55108, MN, United States
[e] Department of Land Surveying and Geo-Informatics, The Hong Kong Polytechnic University, Hong Kong, China

ARTICLE INFO

Keywords:
Cropped field
Smallholder agriculture
Sentinel-1
Sentinel-2
Cropland abandonment
Comparative temporal variation

ABSTRACT

Detailed and updated maps of actively cropped fields on a national scale are vital for global food security. Unfortunately, this information is not provided in existing land cover datasets, especially lacking in smallholder farmer systems. Mapping national-scale cropped fields remains challenging due to the spectral confusion with abandoned vegetated land, and their high heterogeneity over large areas. This study proposed a large-area mapping framework for automatically identifying actively cropped fields by fusing Vegetation-Soil-Pigment indices and Synthetic-aperture radar (SAR) time-series images (VSPS). Three temporal indicators were proposed and highlighted cropped fields by consistently higher values due to cropping activities. The proposed VSPS algorithm was exploited for national-scale mapping in China without regional adjustments using Sentinel-2 and Sentinel-1 images. Agriculture in China illustrated great heterogeneity and has experienced tremendous changes such as non-grain orientation and cropland abandonment. Yet, little is known about the locations and extents of cropped fields cultivated with field crops on a national scale. Here, we produced the first national-scale 20 m updated map of cropped and fallow/abandoned land in China and found that 77 % of national cropland (151.23 million hectares) was actively cropped in 2020. We found that fallow/abandoned cropland in mountainous and hilly regions were far more than we expected, which was significantly underestimated by the commonly applied VImax-based approach based on the MODIS images. The VSPS method illustrates robust generalization capabilities, which obtained an overall accuracy of 94 % based on 4,934 widely spread reference sites. The proposed mapping framework is capable of detecting cropped fields with a full consideration of a high diversity of cropping systems and complexity of fallow/abandoned cropland. The processing codes on Google Earth Engine were provided and hoped to stimulate operational agricultural mapping on cropped fields with finer resolution from the national to the global scale.

1. Introduction

Agriculture is expected to provide increasing food to feed the projected population growth by 2050 (Zabel et al., 2019). Spatially explicit information on cropland as well as the extent of actively cropped fields is critical to understanding its impacts on global food security (Waha et al., 2020). Cropland distribution in the world has experienced tremendous changes in the past decades and will continue in many parts of the world (Qiu et al., 2020a; Olsen et al., 2021). Changes in cropland might introduce significant consequences on agricultural production and ecosystems (Zabel et al., 2019). Cropland abandonment is widely spread and knowledge of its distribution is extremely important for implementing sustainable agricultural management (Tong et al., 2020). It is very important to provide an accurate map of actively cropped fields

* Corresponding author.
E-mail address: qiubingwen@fzu.edu.cn (B. Qiu).

https://doi.org/10.1016/j.jag.2022.103006
Received 26 May 2022; Received in revised form 28 August 2022; Accepted 29 August 2022
Available online 7 September 2022
1569-8432/© 2022 The Authors. Published by Elsevier B.V. This is an open access article under the CC BY-NC-ND license (http://creativecommons.org/licenses/by-nc-nd/4.0/).

across large spatial domains (Wallace et al., 2017). However, information on fallow/abandoned land is currently lacking in existing related literature/datasets (Grogan et al., 2022). The defined cropland in existing land cover products did not provide data on cropping practices such as the basic information on cropped or fallow/abandoned areas (Weiss et al., 2020). Cropped fields are not equivalent to cropland, which may or may not be cultivated with crops during a given year (Siebert et al., 2010). Till now, updated national-scale data on the actively cropped area with the finer resolution are rare and limited in a few developed countries with intensive ground-truth data (Blickensdörfer et al., 2022).

Distinguishing actively cropped fields from fallow/abandoned land is pre-required and hard in agricultural remote sensing applications (Estel et al., 2015; Rufin et al., 2022). In the cropping intensity mapping community, deriving actively cropped fields was widely implemented based on the annual maximum Vegetation Indices (VI) values (Gray et al., 2014; Liu et al., 2021). It is generally assumed that cropped fields show higher VI than the fallow or abandoned cropland (Alcantara et al., 2012). However, the VI temporal profiles in cropped or abandoned cropland show spatiotemporal heterogeneity corresponding to the diversity of local biophysical conditions, and land management (Qiu et al., 2017b; Grădinaru et al., 2019). Mapping cropland abandonment was commonly carried out under the framework of Land Use and Cover Changes (LUCC) (Estel et al., 2015; Zhu et al., 2021). Most studies considered the coverages of barren/grass on former cropland as fallow/abandoned cropland (Zhu et al., 2021). However, besides the herbaceous vegetation communities, there could be woody encroachment (shrubs and trees) following cropland abandonment (Yin et al., 2018). Till now, there are still no reported official statistics on abandoned croplands except for Japan (Li and Li, 2017).

Agricultural mapping is far more complex than broad land cover classification (Gella et al., 2021). There are at least two major challenges in accurately deriving actively cropped fields from cropland on a national scale. The biggest challenge is the spectral similarity between cropland and grassland (Rose et al., 2021). Classification errors are notably introduced by the spectral similarity between crops and other herbaceous classes (Yin et al., 2018). The mapping accuracy of existing cropland products is relatively low due to its high landscape heterogeneity and spectral confusion with grasslands (Nabil et al., 2020). Another great challenge is the spatiotemporal heterogeneity of cropped or fallow/abandoned land across different regions (Blickensdörfer et al., 2022). When cropland was left fallow or abandoned, it would be covered by bare land, grass, or woody plants (shrubs and trees) depending on the biophysical conditions and duration of abandonments (Wang et al., 2016). Most previous studies characterized cropped or fallow/abandoned land by exploring the phenological patterns based on VI time series from MODIS or Landsat images (Estel et al., 2015; Grădinaru et al., 2019). It is difficult to accurately map cropped fields merely by applying the commonly applied VI time series due to the following two kinds of misclassifications: one is the underestimation of cropped fields when the crop biomass is low (i. e. crops cultivated in less favorable biophysical conditions or poorly managed regions) (Rose et al., 2021); the other is the overestimation of cropped fields when the grass biomass in fallow/abandoned cropland is high (Samasse et al., 2018). Automatic agricultural mapping approaches with robust spatiotemporal generalization capabilities are urgently needed (Ge et al., 2021).

The need for mapping cropland consistently over large spatial domains without calibrations calls for automated knowledge-based approaches (Persello et al., 2019). Besides the commonly-applied VI-based approaches, recent studies found that the variations of Synthetic Aperture Radar (SAR) data were efficient in capturing crop management activities such as planting and harvesting (Whelen and Siqueira, 2018; Huang et al., 2021). However, the confusion between grass and crops could not be solved merely by applying SAR data (Huang et al., 2021). Fusing optical and radar images improved classification accuracy in mapping different crop or vegetation types (Chakhar et al., 2021). The launch of Sentinel-1 (S1) and Sentinel-2 (S2) (5 days revisit, 10 or 20 m) provides great opportunities for agricultural monitoring at finer resolutions (Holtgrave et al., 2020). Sentinel-2 MultiSpectral Instrument (MSI) data provide valuable information on leaf pigment, water content, and plant growth status with the unique red-edge bands (Orynbaikyzy et al., 2020). Agricultural land uses can be better characterized by combining vegetation, soil, water, and pigment indices (Qiu et al., 2015; Liu et al., 2020; Qiu et al., 2021). However, to our knowledge, there is a deficiency of automatic mapping algorithms for deriving national-scale cropped fields without regional adjustments by taking full advantage of S1 and S2.

This study aimed to fill this gap by proposing a novel framework for robust mapping actively cropped fields in China using optical and radar time series images. China is dominant by smallholder agriculture and needs to feed the largest population in the world (Lowder et al., 2016). Yet much remains unknown about the traditional large agricultural country, such as the basic information on the total amount of cropped area as well as its spatial distributions at a finer resolution (i. e. 10 m or 20 m). Accurately mapping cropped fields in China is extremely challenging due to the tremendous heterogeneity across different regions and spectral confusion among cropped and fallow/abandoned land (Fig. 1). This study will cope with these challenges and provide the first 20-m cropped fields map and explore the spatial patterns of cropped ratio in China in 2020. Specifically, we address the following questions:

1. How can we depict cropped fields with the full considerations of a high diversity of cropping systems and complexity of cropland abandonments by fusing S1 and S2?

2. What is the cropped ratio in China and the possible discrepancies with the VI_{max} based approaches?

3. How does the cropped ratio vary across different regions and why?

2. Study area and data sources

2.1. Study area

China covers a large range of altitudes and climatic regions. There are north–south contrasts in the climatic and topographic conditions. Southern China is characterized by mountainous and hilly cropland located in favorable climatic conditions (Fig. 1, Fig. S1). Northern China is depicted as a plain or plateau cropland located in Arid and semi-arid regions (Fig. 1). Agriculture in China illustrated great heterogeneity given its high diversity of climate, topography, and cropping systems (Qiu et al., 2017a). China has a complex cropping system and a high crop diversity (Qiu et al., 2018). Multiple cropping is widely implemented in China (Qiu et al., 2022). Agriculture in China has experienced tremendous agricultural structural changes (i.e. non-grain orientation) and widespread cropland abandonment (Ma et al., 2020). Cropland abandonment has emerged as a prevalent phenomenon in China (Qiu et al., 2020b).

2.2. Remote sensing time-series datasets and other datasets

2.2.1. Sentinel-1 SAR images and preprocessing

This study applied both the SAR and optical time-series images. The SAR images used in this study are the Sentinel-1 (S1) data. We applied the Interferometric Wide Swath (IW) instrument mode with dual-band cross-polarization (VV). We utilized all available level-1 Ground Range Detected (GRD) products in China, which included 18417 Sentinel-1 GRD images in 2020. This study developed the smoothed 12-days VV backscattering coefficients time series with Whittaker Smoother (WS) (lambda = 1, order = 2) (Eilers, 2003).

2.2.2. Vegetation, soil, and pigment indices time series based on Sentinel-2 MSI images

All available Level-1C Sentinel-2A/B images were collected, and there were 176604 Sentinel-2 Multi-Spectral Instrument (MSI) images in

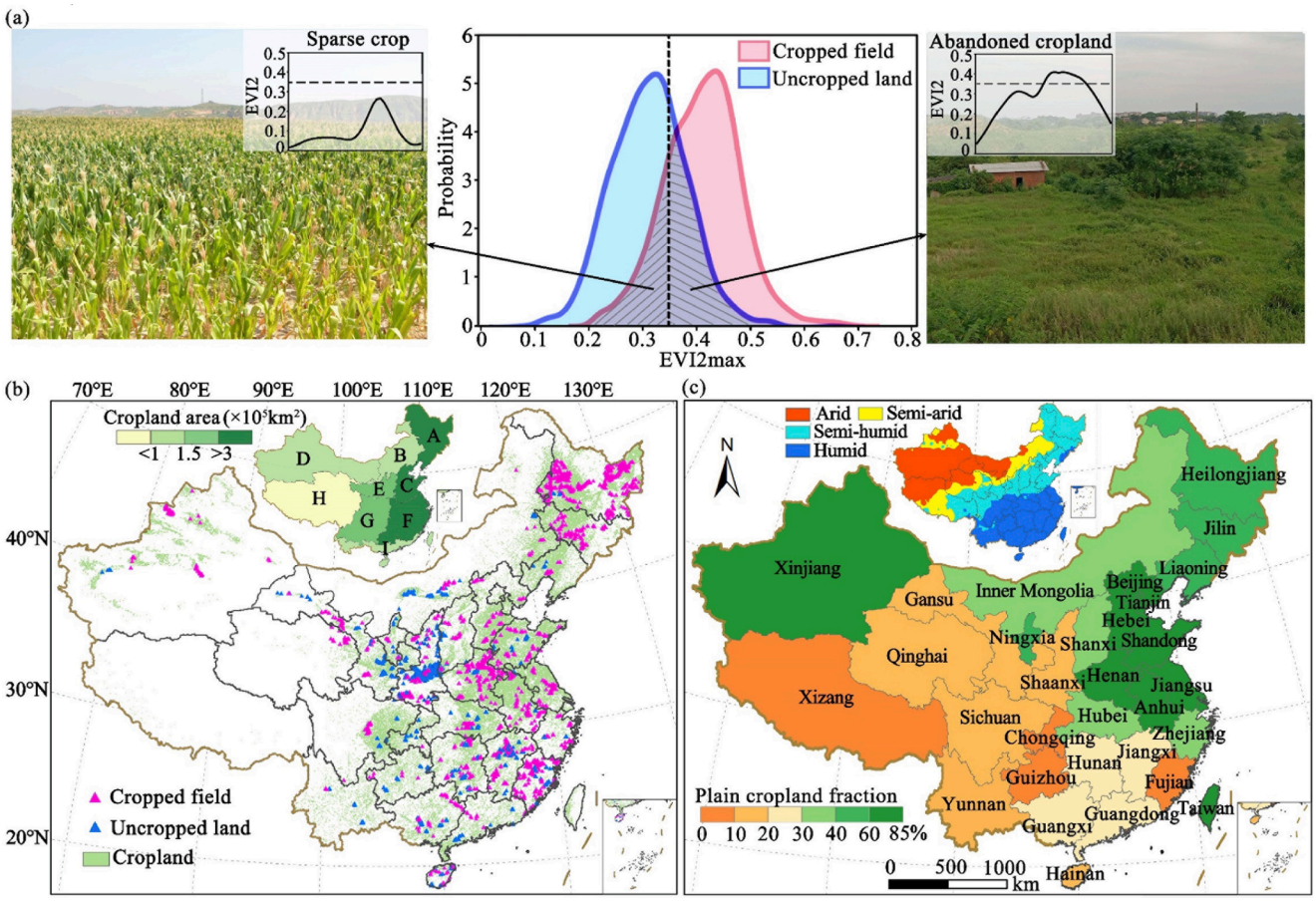

Fig. 1. Maps of (a) density of annual maximum of the two-band Enhanced Vegetation Index (EVI2), field photos and its corresponding EVI2 profiles from cropped fields and uncropped land; (b) reference sites and cropland area of 9 agricultural regions; (c) plain cropland fraction at provincial level & climatic regions.

China in 2020. Spectral indices of vegetation, soil and pigment were computed to characterize cropped fields from multiple dimensions. These three spectral indices were the EVI2 (Jiang et al., 2008), Dry Bare-Soil Index (DBSI) (Rasul et al., 2018) and the Chlorophyll (Chl) Index red edge (CIre) (Gitelson et al., 2005). Larger values in EVI2, DBSI and Chl suggest higher vegetation density, more soil bareness or stronger chlorophyll concentration. The smoothed 10-day composite time series of spectral indices were obtained through discarding the observations of cloud contaminations and smoothed with the Whittaker Smoother (WS) (lambda = 10, order = 2) (Eilers, 2003).

2.2.3. Ground truth references datasets and other datasets

Ground truth reference datasets are vital for algorithms validation in remote sensing application fields. A total of 7,052 ground-truth reference sites were gathered in major agricultural regions in China (Fig. 1). There were 5,548 cropped and 1,504 fallow/abandoned sites, respectively (Table S1). Around 30 % of reference sites (2,118) were applied for determining the thresholds of the VSPS algorithm, and the remaining 70 % (4,934 sites) were exploited for accuracy assessments. Detailed descriptions of collected reference sites were provided in Table S1. The cropland distribution data was derived from the GlobelLand30 datasets in 2020 (Fig. 1), which is the first 30 m resolution global land cover data set with good accuracy (Chen et al., 2015). The topography map (Cheng et al., 2011) was applied to explore the influences of landform types on cropped ratios (Fig. S1).

3. Methodology

This study developed a novel framework for mapping cropped fields by integrating Vegetation, Soil, and Pigment indices from Sentinel-2 and Sentinel-1 SAR time-series images (VSPS) (Fig. 2). Cropped fields are defined as the agricultural area under active cultivation with field crops (i.e. rice, maize, wheat and soybean) during a given year (Smith, 2019). Cropped fields are distinct from cropland, which may be fallow/abandoned for a specific year. The key procedures of the proposed framework included characterizing herbaceous and woody plants, and depicting cropped fields through developing three knowledge-based temporal indicators (the processing codes in provided in Table S2). The first indicator was developed based on Sentinel-1 SAR images, which was proved to be efficient in separating herbaceous and woody plants in related studies (Huang et al., 2021). The latter two indicators were proposed based on Sentinel-2 MSI images, which further extract cropped fields from herbaceous plants. All the procedures were implemented in the Google Earth Engine (GEE) platform. Detailed descriptions were provided as follows.

3.1. Characterizing herbaceous and woody plants based on the S1 time series

3.1.1. Temporal profiles of VV backscatter from the crop, grass, and woody plants

The temporal profiles of Sentinel-1A VV backscatter of different vegetation covers are provided based on selected ground truth reference sites (Fig. 3). The VV backscatter of woody plants fluctuates between −11 bB and −9 bB, which is more stable and higher than other vegetation covers. Crop sites are characterized by VV increasing as a consequence of crop growth in the vegetative period and VV decreasing during the end of the growing season, which is reported in related

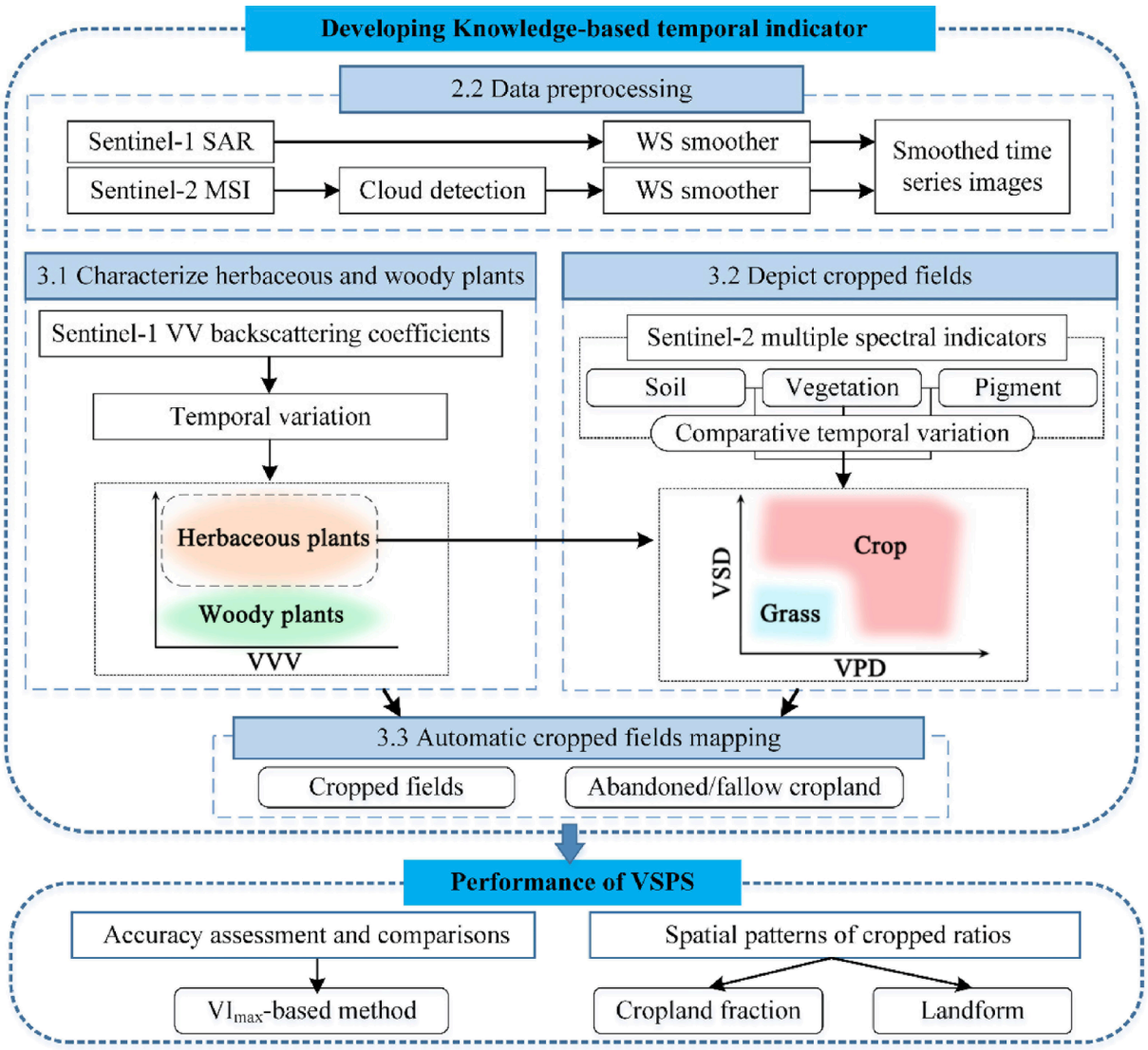

Fig. 2. The overall workflow of the proposed framework for mapping cropped fields. Notes: WS denoted Whittaker Smoother; VVV, VSD and VPD represented the VV-based temporal Variance, Vegetation-Soil Differenced temporal variation and the Vegetation-Pigment Differenced temporal variation, respectively.

studies (Chakhar et al., 2021). All cropped sites were highlighted by the greater dynamic ranges of backscatter than woody plants, which might also be observed in some herbaceous sites of grass (Fig. 3).

3.1.2. *Designing indicator based on the temporal variance of VV backscatter*

The first temporal indicator, the VV-based temporal Variance (VVV), was developed based on the radar VV time series from S1 datasets. The indicator of VVV was defined as:

$$VVV = \frac{\sum_{t=1}^{N}(VV^t - \overline{VV})^2}{N-1} \quad (1)$$

Where denoted the values of VV at temporal composite t, respectively; $\overline{VV}$ indicated the mean values of the VV time series; N is 31 within one year given the temporal resolution of 12 days.

3.2. *Depicting cropped fields based on vegetation, soil, and pigment indices from the S2 time series*

3.2.1. *Similarities and fundamental differences between cropped and uncropped fields*

Vegetation indices alone are not sufficient to fully characterize cropped fields. There exists tremendous heterogeneity in the VI temporal profiles of cropped fields (i.e. the number and magnitudes of VI peaks) given the complexity of cropping patterns, biophysical conditions, and local management activities (Fig. 4). The annual maximum VI values of the cropped and uncropped sites are mixed (Fig. 1). Fallow/abandoned (uncropped) sites could be covered by sparse/dense grass or woody plants. Specifically, there are some sparse crops with unexpectedly low peak VI (i.e. EVI2 less than 0.35) as well as dense grass or woody plants with high peak VI (Fig. 4, Fig. S2).

The incorporation of soil and pigment indices can improve the identification of cropped fields. For cropping sites, the soil index of DBSI often illustrates a rapid increase around the start and end of the crop growing season due to plowing and harvesting activities. However, paddy rice generally illustrates a less obvious surge due to the unique cultivation habit of flooding and transplanting (Fig. 4). Similar to cropped fields, dense grass and woody plant generally show high chlorophyll (CIre) values (Fig. 4).

Despite the similarities, there are some fundamental differences between the cropped and uncropped fields. The fallow/abandoned lands are not subject to any farming activities such as plowing, sowing, irrigation, fertilization, and harvesting. Vegetation covers in fallow/abandoned lands are generally not cleared for the whole year. Therefore,

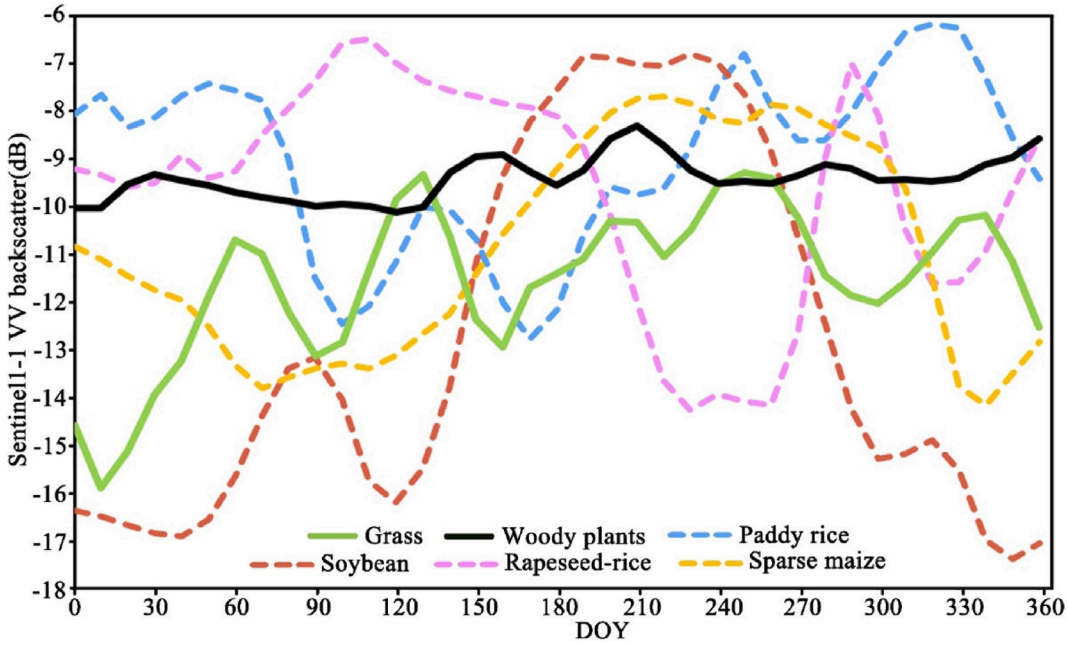

Fig. 3. Temporal profiles of the Sentinel-1 VV backscatter from different vegetation covers.

fallow/abandoned lands are characterized by smooth temporal profiles of vegetation, soil, and chlorophyll indices. Farming activities in cropped fields lead to irregular and abrupt changes in any of the Vegetation-Soil-Chl indices. For example, sparse crops illustrate larger temporal variations in the Chl index despite lower VI values (Fig. 4).

3.2.2. *Designing indicators by exploring comparative temporal variations in Vegetation-Soil-Chl indices*

Besides the VVV indicator from Sentinel-1 data, the cropped fields can be further characterized by exploring the comparative temporal variations in Vegetation-Soil-Chl indices using Sentinel-2 images (Fig. 5). Two temporal indicators were designed by coupling vegetation, soil, and pigment indices. One is the Vegetation-Soil Differenced temporal variation (VSD), and the other is the Vegetation-Pigment Differenced temporal variation (VPD). The VSD is proposed to highlight the rapid unsynchronous comparative changes in slopes of vegetation and soil indices among cropped fields, which is based on the first-order differenced time series between vegetation and soil indices. The VPD is developed to characterize the great unsynchronous comparative changes in the curvature of vegetation and pigment indices, which is based on the second-order differenced time series between vegetation and pigment indices. The functions of these two indicators were provided as follows.

$$VSD = \frac{\sum_{t=1}^{N-1}\left(\left|\left(EVI2^{t+1} - DBSI^{t+1}\right) - \left(EVI2^{t} - DBSI^{t}\right)\right| - Mean_{DED}\right)^2}{N-1} \tag{2}$$

$$VPD = \sum_{t=1}^{N-2}\left|\left(\left(EVI2^{t+2} - CIre^{t+2}\right) - \left(EVI2^{t+1} - CIre^{t+1}\right)\right) - \left(\left(EVI2^{t+1} - CIre^{t+1}\right) - \left(EVI2^{t} - CIre^{t}\right)\right)\right| \tag{3}$$

where, $DBSI^t$ and $CIre^t$ denoted the values of Enhanced Vegetation Index (EVI2) (Jiang et al., 2008), Dry Bare-Soil Index (DBSI) (Rasul et al., 2018), and Chlorophyll (Chl) Index red edge (CIre) (Gitelson et al., 2005) at temporal composite t, respectively; $Mean_{DED}$ represented the mean value of the Differenced time series of EVI2 and DBSI (DED); N is 36 within one year given the temporal resolution of 10 days.

3.3. *Automatic cropped fields mapping based on knowledge-based identification rules*

The first indicator (VVV) based on S1 can efficiently separate woody plants since woody plants generally show lower values in VVV compared to herbaceous plants. The latter two indicators based on S2 (VSD and VPD) further discriminate cropped fields from fallow/abandoned land. The cropped fields obtained greater values in at least either of these latter two indicators (VSD and VPD) (Fig. 6). For example, sparse crop often shows high values in VSD and VPD than other herbaceous plants (sparse or dense grass). Specifically, sites from multiple cropping or dry crops generally display greater values in VSD and VPD than single cropping, paddy fields and sparse crops (Fig. S2). In contrast, the fallow/abandoned cropland consistently illustrate lower values in these latter two indicators based on S2 (VSD and VPD), despite possible high values in spectral indices of EVI2 or CIre (i.e. dense grass). Therefore, a simple decision rule could be exploited to highlight cropped fields using these three developed indicators.

$$if\,(VVV > \theta_1)\ and\ ((VSD > \theta_2)\ or\ (VPD > \theta_3)),\ Cropped = 1; else\ Cropped = 0 \tag{4}$$

where,θ_1,θ_2 and θ_3 are constant; VSD, VPD, and VVV represented the indicators designed based on vegetation & soil, vegetation & pigment, and VV backscatter time series, respectively. This algorithm was implemented to cropland pixels in China through a per-pixel strategy.

3.4. *Performance evaluations of the VSPS algorithm*

Accuracy assessment of agricultural remote sensing classification results can be conducted using the agricultural statistical data, reference data from field surveys, and interpreted from higher-resolution images. However, there was no officially reported data on the amounts of cropped fields in China. Cropped ratios can be calculated based on agricultural statistical data and exploited to evaluate the rationality of the remote sensing estimated results in single-cropping regions (only several provinces in northern China). Therefore, validation of the proposed VSPS algorithm was conducted based on the reference sites described in section 2.2.3. The reference sites were applied to calculate the confusion matrix following the best practices method (Olofsson

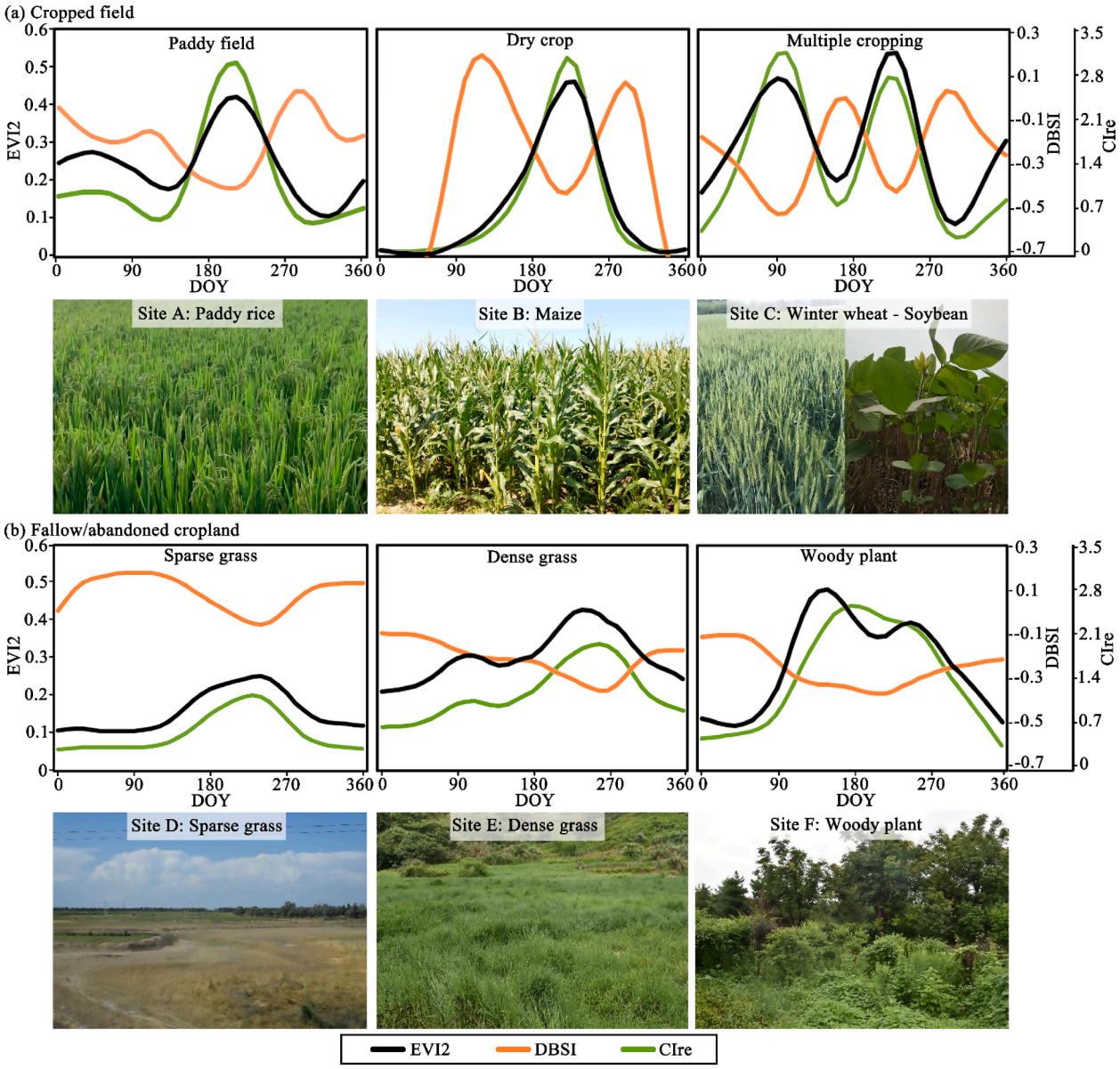

Fig. 4. Temporal profiles of EVI2, DBSI and CIre from (a) cropped fields and (b) fallow/abandoned lands. Notes: Site A: Paddy rice in Fujian province, 118°29′49″, 25°49′51″; Site B: Maize in Heilongjiang province, 116°43′31″, 24°45′23″; Site C: Winter wheat-Soybean in Henan province, 115°5′6″, 34°42′17″; Site D: Sparse grass in Inner Mongolia province, 121°38′15″, 45°11′56″; Site E: Dense grass in Guangdong province, 110°34′39″, 21°29′35″; Site F: Woody plant in Hunan province, 113°37′19″, 28°7′50″. Notes: DOY represents the day of the year.

et al., 2014) to evaluate the cropped fields map estimated by the VSPS method. The user's, producer's, and overall accuracies, the kappa index, and F_1 score are calculated to assess the mapping accuracy (Hripcsak and Rothschild, 2005). The performance evaluations of the VSPS algorithm were further conducted through its comparisons with the commonly applied VImax-based method. The spatial patterns of cropped ratios at different agricultural regions/provinces were analyzed and their relationships with cropland fractions and landforms were investigated.

4. Results

4.1. Map of cropped and fallow land of China in 2020

There are distinctive north–south trends in the distribution maps of these three designed temporal indicators (VVV, VSD, and VPD) (Fig. 6). These three designed indicators were efficient in characterizing cropped and fallow lands (Fig. 6). Cropped fields were distinguished by higher values in these three indicators (Fig. 6). Uncropped fields consistently illustrated lower values in these three indicators. Especially, grass illustrated the lowest values in the two indicators based on S2 MSI images (Fig. 6). These three proposed indicators could efficiently distinguish cropped fields from fallow/abandoned land, since cropped fields obtained higher values in these three indicators (Fig. 6 (d, e)).

The first national map of cropped fields with a finer spatial resolution (20 m) in China in 2020 was achieved using the proposed VSPS algorithm (Fig. 7). The thresholds in the decision rule were determined by the training samples described in section 2.2.3. The values of θ_1,θ_2 and θ_3 were decided as 1, 0.001 and 0.8, respectively (Fig. 6). The thresholds were applied to the national scale without additional regional adjustments. Around 151.23 million hectares of land are actively cropped in China in 2020, which is primarily distributed in the north portion of China (Fig. 8). Cropped fields accounted for less than four-fifths (77.07 %) of croplands on a national scale. The cropped ratios showed obvious

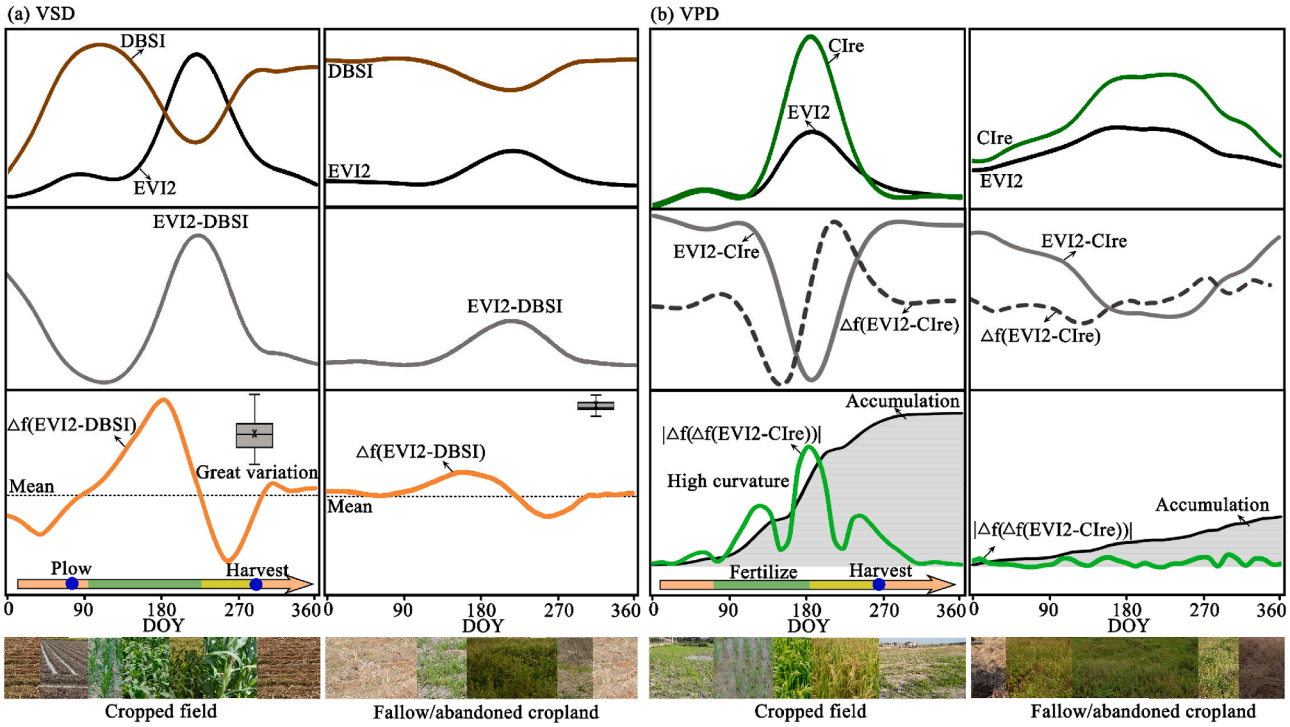

Fig. 5. Developing temporal indicators based on vegetation, pigment and soil indices: (a) VSD; (b) VPD. Notes: △f(EVI2-DBSI), △f(EVI2-CIre) represented the first-order differenced time series of EVI2-DBSI and EVI2-CIre, respectively. △(△f(EVI2-CIre)) denoted the second-order differenced time series of EVI2-CIre. The boxplots represented the statistical distributions of △f(EVI2-CIre) in the study year.

spatial heterogeneity among different agricultural regions/provinces (Fig. 7, Fig. S3). The highest cropped ratio was examined in region A, followed by regions B, C, D, E, F, G, H, and I (Fig. S3). Specifically, the cropped ratio in Northeast China (region A) was roughly 100 % (97 %), in contrast to lower than 60 % (56.87 %) in South China (region I) (Fig. 7, Fig. S3).

4.2. Accuracy assessment of the cropped fields map

Accuracy assessments were conducted based on reference sites (Table 1). The overall accuracy was 94.04 % and the kappa index was 0.8275. Among these 3,880 sites of cropped fields, 3,692 sites (95.15 %) were correctly labeled. Among 1,054 sites of uncropped fields, 948 sites (89.94 %) were accurately identified. The producer accuracy of uncropped fields significantly improved through the incorporation of two temporal indicators (VSD, VPD) based on Sentinel-2 MSI images (Table S3). The indicator of VVV cannot efficiently separate crops from grass. Around one-half of the grass sites were misclassified as cropped fields if only the indicator VVV was applied for mapping (Table S4). The proposed VSPS algorithm can efficiently label sparse crops and separate grass from cropped fields (Fig. 7, Fig. S3).

4.3. Spatial pattern of estimated cropped ratios and comparisons with other approaches

The cropped ratios illustrate latitudinal gradients, which declined from the north to the south (Fig. 8, Fig. S3). The whole country can be divided into three portions by two altitudinal lines (32 and 38°) for simplification. The cropped ratio was 92 % in the north, dropped to 80 % in the middle, and 59 % in the south. At the provincial level, the cropped ratio declined from 98 % in Heilongjiang to 35 % in Xizang province (Fig. 8, Table S5). Cropped ratios estimated by the VSPS algorithm were highly associated with the types of landform, which declined from 84 % in plain to 63 % in the mountain (Fig. 8). At the provincial level, the percentage of plain cropland accounted for roughly-one-half of the variations in cropped ratios (Fig. 8). The cropped ratio was positively associated with cropland fraction at 1 km resolution and cropland per agricultural population (Fig. 8, Fig. S4). The cropped ratios consistently enhanced with the cropland fraction among different landforms, with more distinctive differences in plains (Fig. 8).

The performance of the proposed VSPS algorithm was compared to the commonly applied VImax-based method. In the agricultural remote sensing research communities, the maximum VI-based strategy was generally applied to identify the crop growth cycles. Specifically, pixels with higher annual maximum of Normalized Difference Vegetation Index (NDVI) or EVI2 values (i.e. $NDVI_{max} > 0.5$ or $EVI2_{max} > 0.35$) were labeled as cropped areas (Gray et al., 2014). Compared to the proposed VSPS algorithm, the VImax-based method approaches obtained much lower accuracy (overall accuracy less than 80 %) (Table 1). Additionally, there are tremendous discrepancies in estimated cropped ratios by the maximum VI-based strategy using different datasets: around 60 % based on Sentinel-2 MSI images in contrast to around 90 % based on MODIS images on a national scale (Fig. 8, Table S5). Obvious commission errors of the MVIM approach were confirmed from the ground truth reference sites, especially in southern mountainous and hilly regions (Fig. 7, Fig. S3). A majority of the uncropped sites (758 out of 1054 sites) were incorrectly identified as cropped sites (Table 1). There were distinctive omission errors for the MVIS approach (Fig. 7, Table 1), which were primarily introduced by sparse crops in northern China (Fig. 7, Fig. S3). The sparse crops are widely distributed in cropped fields with unfavorable climatic (i.e. arid or semi-arid regions) or soil conditions (Fig. S1). For example, the cropped ratio by MVIS in Inner Mongolia was only 55 %, which was roughly-one-half lower than that reported by the agricultural statistical data (97 %) (Table S6). It sounded unreasonable that cropped ratios were considerably higher or the highest (by MODIS images) in mountains when estimated by the maximum VI-based strategy (Fig. 8(c)).

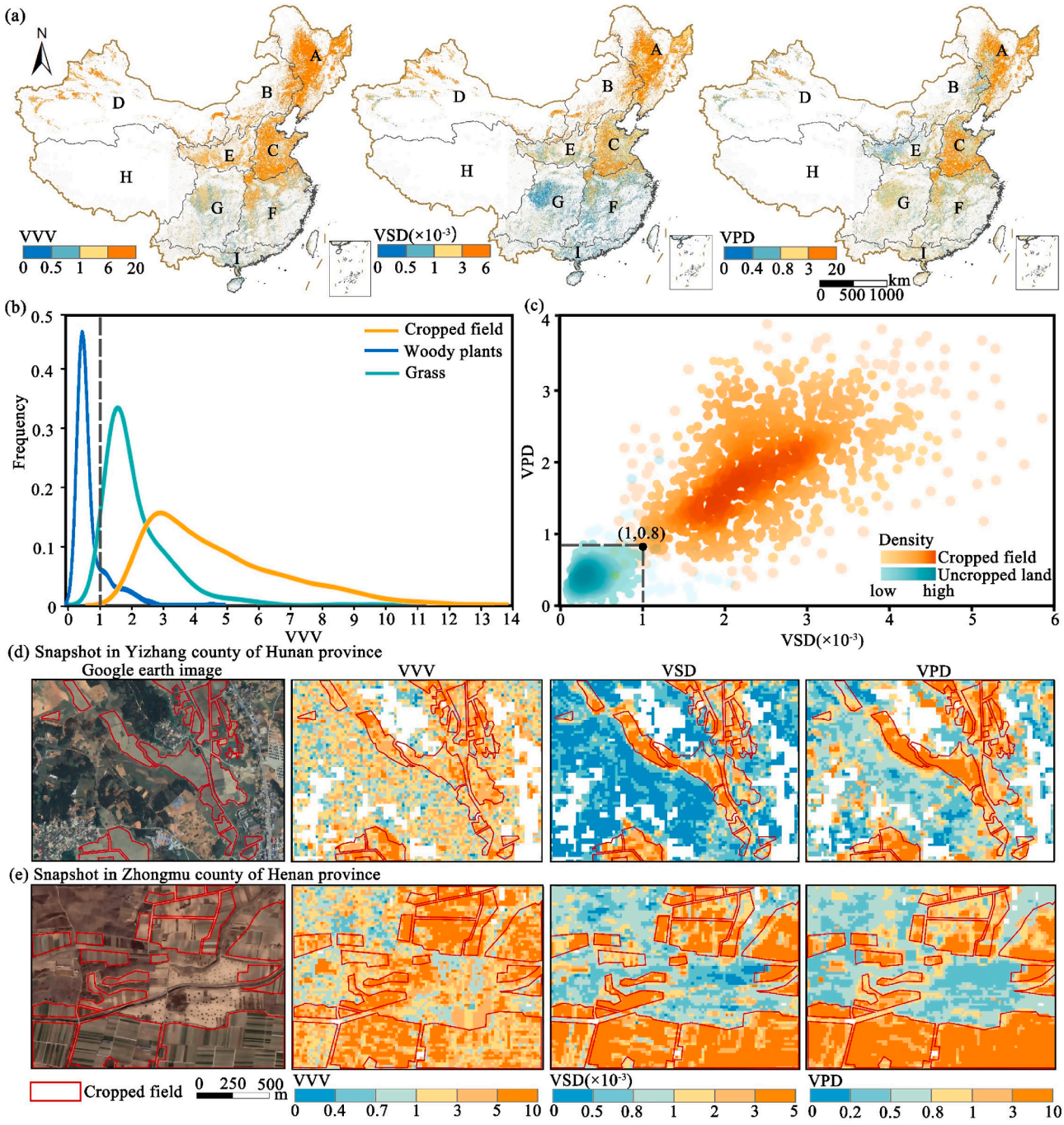

Fig. 6. Maps of (a) three temporal indicators (VVV, VSD, VPD), (b) the density map of VVV, (c) scatter plot between VSD and VPD and some snapshots in (d) Yizhang county of Hunan province and (e) Zhongmu county of Henan province.

5. Discussion

There is a deficiency of efficient algorithms for mapping actively cropped fields across large spatial domains, especially in smallholder agricultural systems on a national scale (Bégué et al., 2018). The commonly applied VImax-based approach is associated with uncertainties or even serious classification errors in the following three aspects. The first kind of uncertainty is associated with the high spatial heterogeneity of croplands across large regions (Ashourloo et al., 2022). This kind of uncertainty is typically illustrated by omission errors in the case of sparse crops (Fig. S3) (Rose et al., 2021) and overestimation of cropped fields in fallow/abandoned land with favorable biophysical conditions (Grădinaru et al., 2019). For example, the VI_{max} based approach based on MODIS images illustrated very high cropped ratios in southern China, even in mountainous cropland (Fig. 8). The second kind of uncertainty is related to the possible incomparability of calculated VI across different platforms. Especially, there are large discrepancies in cropped ratios when estimated by different datasets such as the Sentinel-2 and MODIS EVI2 images (Fig. 8). The third kind of uncertainty is linked with possible underestimation of cropped fields by VI time series with less valid observations. The the real heading stages of agricultural crops might be missed when estimated by VI data with lower temporal resolution or in regions with regular cloud contaminations (i.e. southern China) (Fig. 8, Fig. S4).

Automatic mapping strategies using knowledge-based features/indices illustrated the significance of simplifications and efficiency

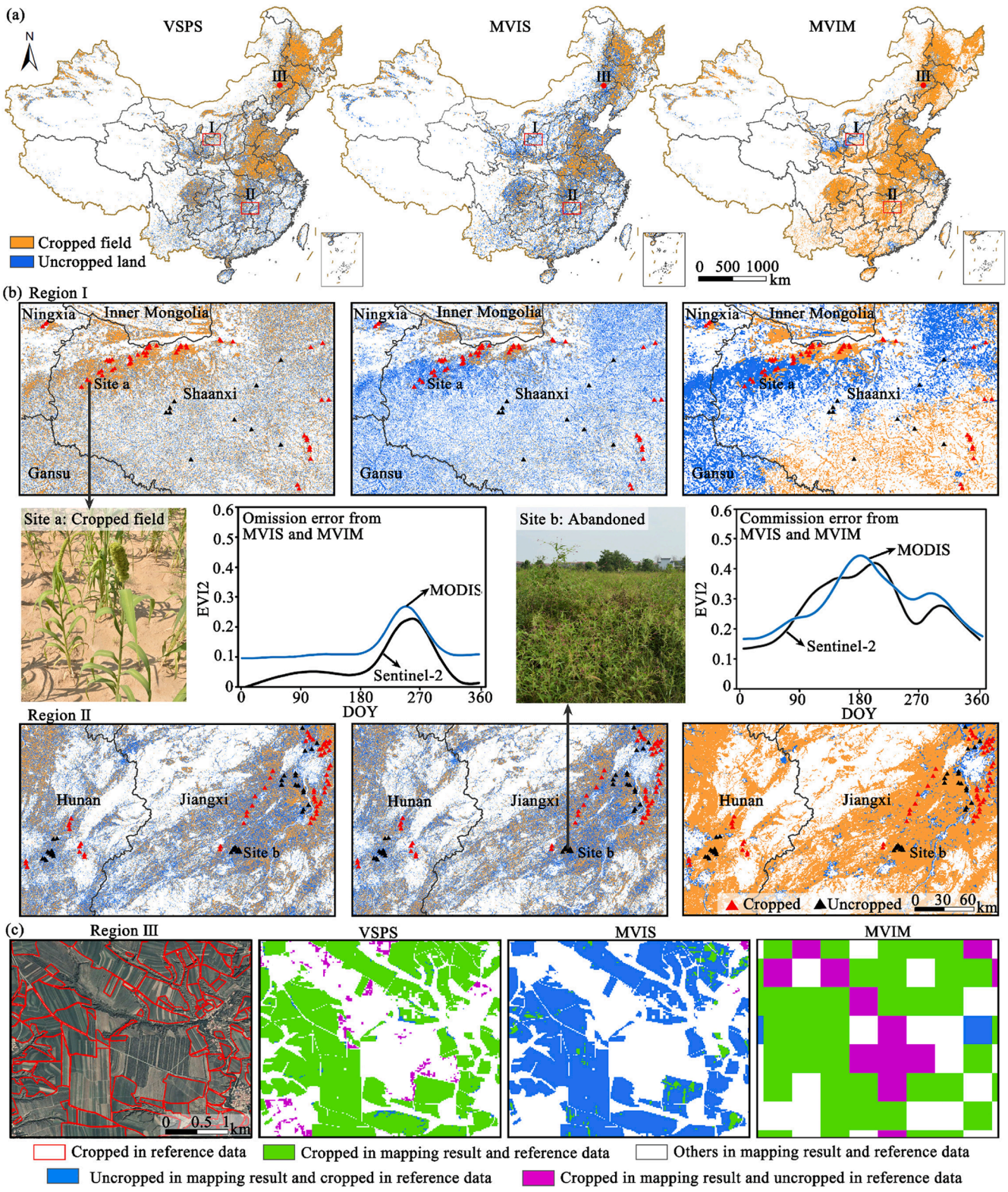

Fig. 7. Comparisons between VSPS method and VI_{max}-based method: (a) distribution maps, and (b, c) some snapshots showing the omission errors in northern China and commission errors in southern China estimated from the VI_{max}-based method. Notes: The VI_{max}-based method included MVIS and MVIM, which represented Maximum VI-based strategy (EVI2 > 0.35) based on Sentinel-2 MSI or MODIS images, respectively. Cropped fields in reference data in region III were visually interpreted based on Google Earth images.

(Waldner et al., 2015). The proposed features/indices highlight the target class such as cropland or crop types by their highest or lowest values (Ashourloo et al., 2020). Temporal features were generally developed based on the vegetation indices and visible bands (i. e. the red band) time series from MODIS or Landsat images (Massey et al., 2017). Recent studies found that the incorporation of other spectral indices such as the soil, water, and pigment indices enhanced the efficiency in agricultural remote sensing applications (Liu et al., 2020; Huang et al.,

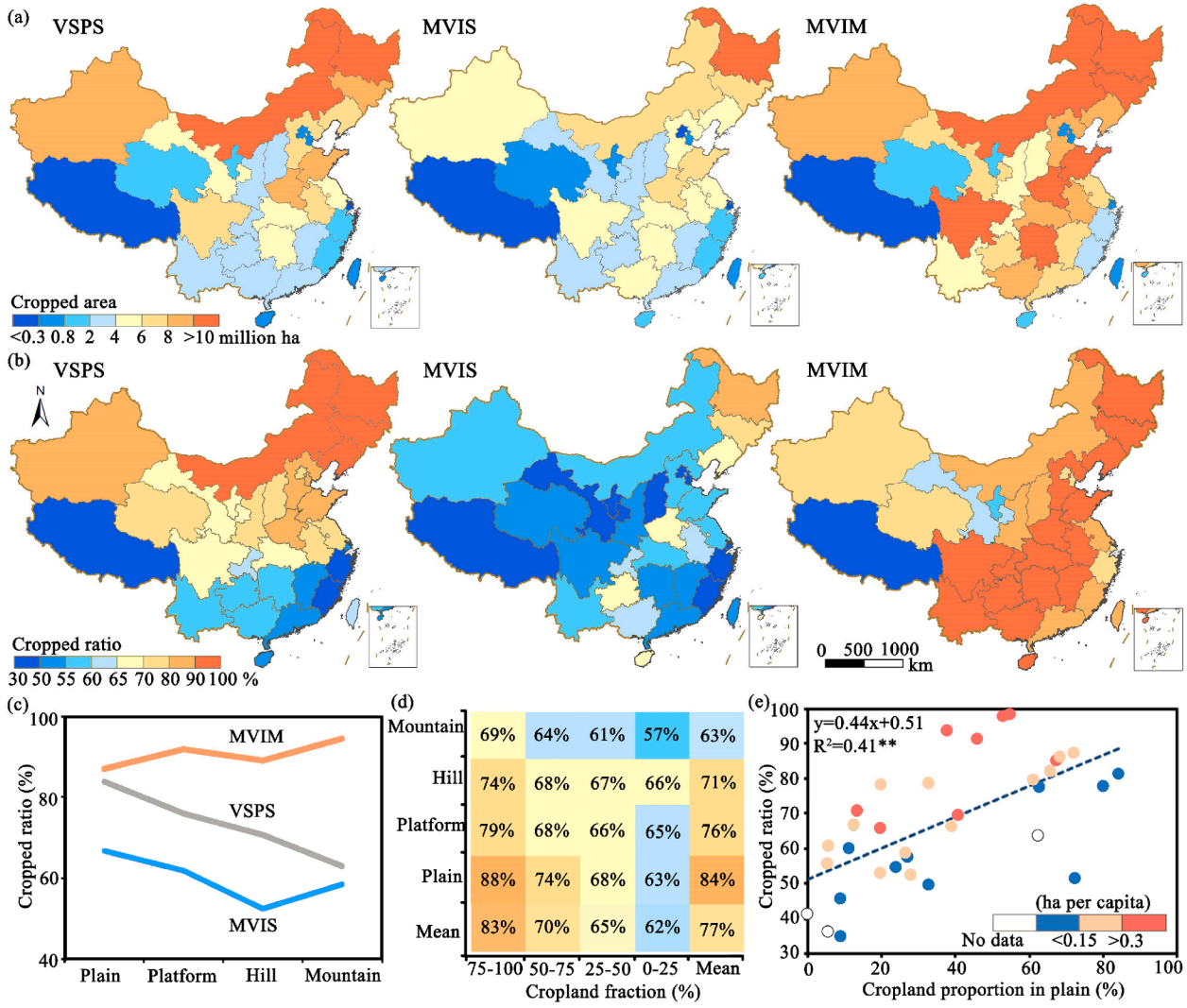

Fig. 8. Maps of (a) estimated cropped areas, (b) cropped ratio at province level, (c) cropped ratio among different landforms from three algorithms, (d) cropped ratio among different landforms together with cropland fraction at 1 km; (e) relationships between cropped ratios and plain cropland percentages at the provincial level. Notes: MVIS and MVIM represented Maximum VI-based strategy based on the Sentinel-2 MSI images or the MODIS images, respectively. The color of sub-figure (e) denoted the cropland per agricultural population (seen Fig. S4).

Table 1
Accuracy assessment based on ground truth reference sites.

	Total	VSPS				MVIS				MVIM			
		Cropped	Others	PA (%)	F1/%	Cropped	Others	PA (%)	F1/%	Cropped	Others	PA (%)	F1/%
Cropped	**3880**	**3692**	**188**	**95.15**	**96.17**	**3183**	**697**	**82.04**	**86.55**	**3608**	**272**	**92.99**	**87.51**
Others	**1054**	**106**	**948**	**89.94**	**86.58**	**292**	**762**	**72.30**	**60.64**	**758**	**296**	**28.08**	**36.50**
UA (%)		**97.21**	**83.45**			**91.60**	**52.23**			**82.64**	**52.11**		
OA (%)		**94.04**				**79.33**				**79.12**			
Kappa		**0.8275**				**0.4766**				**0.2533**			

Notes: PA, UA, and OA represented producer, user, and overall accuracy, respectively. MVIS and MVIM represented Maximum VI-based strategy (EVI2 > 0.35) based on Sentinel-2 MSI or MODIS images, respectively.

2022). Parameters revealing temporal variations (i.e. maximum positive/negative slope, standard derivation, and coefficient of variation) have been proved to be capable of characterizing cropland and crop types (Waldner et al., 2015; Huang et al., 2021).

The proposed VSPS algorithm achieved improved performances through developing knowledge-based temporal features based on comparative temporal variations of multiple indices (Table S3). Cropped fields experience cropping activities such as plowing, fertilization, irrigation, and harvesting (Estel et al., 2015), which will lead to irregular, frequent and unsynchronous changes among vegetation, soil, and pigment indices. These developed indicators (VSD, VPD) can characterize cropped fields by quantifying the comparative changes among multiple spectral indices. The VSPS algorithm avoids commission errors by efficiently separating dense grass from cropped fields. And it also eliminates omission errors by correctly labelling sparse crop with lower VI_{max} values, which is mainly distributed in North China and Northwest China (Fig. 7). The proposed VSPS algorithm achieved promising accuracy even though more than one-half of reference sites were located in

cloudy regions with less than 50 % valid observations (Table S1).

Knowledge-based mapping strategies demonstrated the capabilities of consistent and accurate mapping across different regions (Planque et al., 2021). Knowledge-based temporal features have successfully been applied to build decision rules or train machine learning algorithms to support automated cropland mapping at a large scale (Xiong et al., 2017). The increasing availability of Sentinel-2 MSI and Sentinel-1 SAR time series offers unprecedented opportunities for finer-resolution agricultural land mapping at large spatial domains (Planque et al., 2021). Nevertheless, the potential of fusing SI and S2 in cropped fields mapping has not been fully explored yet (Weiss et al., 2020; Blickensdörfer et al., 2022). Recent research efforts found that changing backscatter responses caused by cropping activities (i.e. planting and harvesting) could be captured by the temporal variations (Coefficient of Variation, CoV) of cross-polarized L-band SAR data from the ALOS PALSAR satellite (Whelen and Siqueira, 2018; Huang et al., 2021). However, merely relying on the temporal variations of SAR images performed badly for separating cropland from grassland/pasture (Rose et al., 2021). The proposed VSPS algorithm achieved robustness and satisfactory accuracy over large areas by fusing the freely accessible S1 and S2 data. The VSPS method achieved superior performances in labelling sparse crops and excluding dense grass, which are major sources of errors in existing approaches that only apply vegetation indices or SAR images. It was successfully exploited for national-scale mapping of complex smallholder agricultures with no need for regional adjustments or additional reference training data for each subregion. Therefore, the proposed VSPS algorithm developed based on GEE is expected to be easily reproducible for global applications.

Updated knowledge of the spatial distribution of actively cropped fields in China is very important to global food security. However, accurate and updated information on actively cropped fields in smallholder agricultural systems with finer resolution is still scarce and not fully explored (Rufin et al., 2022). This study presented the first 20 m national-scale spatiotemporal explicit data of the cropped and fallow/abandoned fields in China, enabled by S1, S2, and GEE engines. We found that over one-fifth of cropland was fallow or abandoned on a national scale and with a higher fallow/abandoned ratio in mountainous counties (Table S5). Results in this study were roughly consistent with a recent related study using a regression model based on socio-economic variables (Li et al., 2018). The estimated cropland abandonment by the VSPS algorithm was much greater than previous studies based on supervised classifiers (Zhu et al., 2021), which did not consider the conversion of cropland into woodland. Cropland abandonment in mountainous and hilly regions is far more than we expected, which are widely reported in recent studies (Shi et al., 2018).

There are several uncertainties. First, the estimated cropped ratios/areas are dependent on the accuracy of cropland datasets. Second, it is challenging to properly define and separate cropped and abandoned land in agricultural remote sensing communities (Alcantara et al., 2012). Underestimation or overestimation of cropped fields might occur in permanent crops with fewer management activities or heavily-grazed fallow fields (Tong et al., 2020). Finally, the mapping accuracy is dependent on the data availability of time series images across different regions (Estel et al., 2015). Frequent cloud contaminations could result in classification errors of the estimated cropped fields (especially omission errors) (Fig. S4) (i. e. southwestern China). Data availability could be improved by fusing more optical images from different platforms such as the Landsat, GaoFen and PlanetScope datasets (Rufin et al., 2022). Future work could be conducted to extend the mapping framework for automatically identifying cropped fields across multiple years with no reference to cropland datasets.

6. Conclusions

This study proposed a knowledge-based framework for mapping cropped fields with finer resolution at a national scale. Cropped fields consistently show large temporal variations caused by cropping activities. The main characteristics of actively cropped land were detected based on the temporal variations of backscatter coefficients and comparative temporal variations of vegetation, soil and pigment indices. The cropped fields consistently show high values in these three proposed knowledge-based temporal indicators. A simple decision rule was developed and applied to identify national-scale cropped fields in China without regional adjustments and additional training. Its capability of automatically mapping actively cropped fields in smallholder farms over large spatial domains was verified based on 4,934 widely spread reference sites. The proposed automated mapping strategy demonstrated superior performances over applying vegetation indices or SAR images solely. The VSPS method was particularly successful in accurately labelling sparse crops and efficiently separating dense grass from cropped fields. We presented the first national-scale 20 m updated map of cropped fields in China and revealed that less than 80 % (77 %) of national cropland was cropped at the national scale. The estimated cropped ratios declined from almost 100 % in some northern provinces to less than 50 % in some southern provinces, which were closely related to landforms, cropland factions, and cropland per agricultural population. The outcomes of this study can support the development of remote sensing mapping strategies for agricultural management activities at a national or even global scale.

Declaration of Competing Interest

The authors declare that they have no known competing financial interests or personal relationships that could have appeared to influence the work reported in this paper.

Data availability

Data will be made available on request.

Acknowledgments

This work was supported by the National Natural Science Foundation of China (grant no. 42171325, 41771468), the Science Bureau of Fujian Province (2020N5002), the Ministry of Natural Resources of China (KY-010000-04-2000-002) and the Fujian provincial department of ecology and environment (2022R023). Thanks to our research group members and collaborators for collecting the ground reference data. We are very grateful to the editors and anonymous reviewers for offering insightful suggestions which significantly improve the manuscript.

Appendix A. Supplementary material

Supplementary data to this article can be found online at https://doi.org/10.1016/j.jag.2022.103006.

References

Alcantara, C., Kuemmerle, T., Prishchepov, A.V., Radeloff, V.C., 2012. Mapping abandoned agriculture with multi-temporal MODIS satellite data. Remote Sens Environ. 124, 334–347.

Ashourloo, D., Shahrabi, H.S., Azadbakht, M., Rad, A.M., Aghighi, H., Radiom, S., 2020. A novel method for automatic potato mapping using time series of Sentinel-2 images. Comput Electron Agr. 175, 105583.

Ashourloo, D., Nematollahi, H., Huete, A., Aghighi, H., Azadbakht, M., Shahrabi, H.S., Goodarzdashti, S., 2022. A new phenology-based method for mapping wheat and barley using time-series of Sentinel-2 images. Remote Sens Environ. 280, 113206.

Bégué, A., Arvor, D., Bellon, B., Betbeder, J., De Abelleyra, D., P. D. Ferraz, R., Lebourgeois, V., Lelong, C., Simões, M. and R. Verón, S., 2018. Remote Sensing and Cropping Practices: A Review. Remote Sensing. 10,99.

Blickensdörfer, L., Schwieder, M., Pflugmacher, D., Nendel, C., Erasmi, S., Hostert, P., 2022. Mapping of crop types and crop sequences with combined time series of Sentinel-1, Sentinel-2 and Landsat 8 data for Germany. Remote Sens Environ. 269, 112831.

Chakhar, A., Hernández-López, D., Ballesteros, R., Moreno, M.A., 2021. Improving the Accuracy of Multiple Algorithms for Crop Classification by Integrating Sentinel-1 Observations with Sentinel-2 Data. Remote Sensing. 13, 243.
Chen, J., Chen, J., Liao, A., Cao, X., Chen, L., Chen, X., He, C., Han, G., Peng, S., Lu, M., 2015. Global land cover mapping at 30 m resolution: A POK-based operational approach. ISPRS J. Photogramm. Remote Sens. 103, 7–27.
Cheng, W., Zhou, C., Chai, H., Zhao, S., Liu, H., Zhou, Z., 2011. Research and compilation of the geomorphologic atlas of the People's Republic of China (1:1,000,000). J. Geog. Sci. 21, 89–100.
Eilers, P.H.C., 2003. A perfect smoother. Anal Chem. 75, 3631–3636.
Estel, S., Kuemmerle, T., Alcántara, C., Levers, C., Prishchepov, A., Hostert, P., 2015. Mapping farmland abandonment and recultivation across Europe using MODIS NDVI time series. Remote Sens Environ. 163, 312–325.
Ge, S., Zhang, J., Pan, Y., Yang, Z., Zhu, S., 2021. Transferable deep learning model based on the phenological matching principle for mapping crop extent. Int. J. Appl. Earth. Obs. 102, 102451.
Gella, G.W., Bijker, W., Belgiu, M., 2021. Mapping crop types in complex farming areas using SAR imagery with dynamic time warping. Isprs J Photogramm. 175, 171–183.
Gitelson, A.A., Viña, A., Ciganda, V., Rundquist, D.C., Arkebauer, T.J., 2005. Remote estimation of canopy chlorophyll content in crops. Geophys Res Lett. 32.
Grădinaru, S.R., Kienast, F., Psomas, A., 2019. Using multi-seasonal Landsat imagery for rapid identification of abandoned land in areas affected by urban sprawl. Ecol Indic. 96, 79–86.
Gray, J., Friedl, M., Frolking, S., Ramankutty, N., Nelson, A., Gumma, M., 2014. Mapping Asian Cropping Intensity With MODIS. IEEE J. Sel. Top. Appl. Earth Obs. Remote Sens. 7, 3373–3379.
Grogan, D., Frolking, S., Wisser, D., Prusevich, A., Glidden, S., 2022. Global gridded crop harvested area, production, yield, and monthly physical area data circa 2015. Sci. Data 9, 15.
Holtgrave, A.-K., Röder, N., Ackermann, A., Erasmi, S., Kleinschmit, B., 2020. Comparing Sentinel-1 and -2 Data and Indices for Agricultural Land Use Monitoring. Remote Sensing. 12, 2919.
Hripcsak, G., Rothschild, A.S., 2005. Agreement, the F-Measure, and Reliability in Information Retrieval. J Am Med Inform Assn. 12, 296–298.
Huang, Y., Qiu, B., Chen, C., Zhu, X., Wu, W., Jiang, F., Lin, D., Peng, Y., 2022. Automated soybean mapping based on canopy water content and chlorophyll content using Sentinel-2 images. Int. J. Appl. Earth. Obs. 109, 102801.
Huang, X., Reba, M., Coffin, A., Runkle, B.R.K., Huang, Y., Chapman, B., Ziniti, B., Skakun, S., Kraatz, S., Siqueira, P., Torbick, N., 2021. Cropland mapping with L-band UAVSAR and development of NISAR products. Remote Sens Environ. 253, 112180.
Jiang, Z., Huete, A.R., Didan, K., Miura, T., 2008. Development of a two-band enhanced vegetation index without a blue band. Remote Sens Environ. 112, 3833–3845.
Li, S., Li, X., 2017. Global understanding of farmland abandonment: A review and prospects. J. Geog. Sci. 27, 1123–1150.
Li, S., Li, X., Sun, L., Cao, G., Fischer, G., Tramberend, S., 2018. An estimation of the extent of cropland abandonment in mountainous regions of China. Land Degrad Dev. 29, 1327–1342.
Liu, L., Xiao, X., Qin, Y., Wang, J., Xu, X., Hu, Y., Qiao, Z., 2020. Mapping cropping intensity in China using time series Landsat and Sentinel-2 images and Google Earth Engine. Remote Sens Environ. 239.
Liu, X., Zheng, J., Yu, L., Hao, P., Chen, B., Xin, Q., Fu, H., Gong, P., 2021. Annual dynamic dataset of global cropping intensity from 2001 to 2019. Sci. Data 8, 283.
Lowder, S.K., Skoet, J., Raney, T., 2016. The Number, Size, and Distribution of Farms, Smallholder Farms, and Family Farms Worldwide. World Dev. 87, 16–29.
Ma, L., Long, H., Tu, S., Zhang, Y., Zheng, Y., 2020. Farmland transition in China and its policy implications. Land Use Policy. 92, 104470.
Massey, R., Sankey, T.T., Congalton, R.G., Yadav, K., Thenkabail, P.S., Ozdogan, M., Meador, A.J.S., 2017. MODIS phenology-derived, multi-year distribution of conterminous U.S. crop types. Remote Sens Environ. 198, 490–503.
Nabil, M., Zhang, M., Bofana, J., Wu, B., Stein, A., Dong, T., Zeng, H., Shang, J., 2020. Assessing factors impacting the spatial discrepancy of remote sensing based cropland products: A case study in Africa. Int. J. Appl. Earth. Obs. 85, 102010.
Olofsson, P., Foody, G.M., Herold, M., Stehman, S.V., Woodcock, C.E., Wulder, M.A., 2014. Good practices for estimating area and assessing accuracy of land change. Remote Sens Environ. 148, 42–57.
Olsen, V.M., Fensholt, R., Olofsson, P., Bonifacio, R., Butsic, V., Druce, D., Ray, D., Prishchepov, A.V., 2021. The impact of conflict-driven cropland abandonment on food insecurity in South Sudan revealed using satellite remote sensing. Nature Food. 2, 990–996.
Orynbaikyzy, A., Gessner, U., Mack, B., Conrad, C., 2020. Crop Type Classification Using Fusion of Sentinel-1 and Sentinel-2 Data: Assessing the Impact of Feature Selection, Optical Data Availability, and Parcel Sizes on the Accuracies. Remote Sensing. 12, 2779.
Persello, C., Tolpekin, V.A., Bergado, J.R., de By, R.A., 2019. Delineation of agricultural fields in smallholder farms from satellite images using fully convolutional networks and combinatorial grouping. Remote Sens Environ. 231, 111253.
Planque, C., Lucas, R., Punalekar, S., Chognard, S., Hurford, C., Owers, C., Horton, C., Guest, P., King, S., Williams, S., Bunting, P., 2021. National Crop Mapping Using Sentinel-1 Time Series: A Knowledge-Based Descriptive Algorithm. Remote Sensing. 13, 846.
Qiu, B., Yang, X., Tang, Z., Chen, C., Li, H. and Berry, J., 2020b. Urban expansion or poor productivity: Explaining regional differences in cropland abandonment in China during the early 21st century. Land Degrad Dev.
Qiu, B., Li, W., Tang, Z., Chen, C., Qi, W., 2015. Mapping paddy rice areas based on vegetation phenology and surface moisture conditions. Ecol Indic. 56, 79–86.
Qiu, B., Lu, D., Tang, Z., Song, D., Zeng, Y., Wang, Z., Chen, C., Chen, N., Huang, H., Xu, W., 2017a. Mapping cropping intensity trends in China during 1982–2013. Appl. Geogr. 79, 212–222.
Qiu, B., Luo, Y., Tang, Z., Chen, C., Lu, D., Huang, H., Chen, Y., Chen, N., Xu, W., 2017b. Winter wheat mapping combining variations before and after estimated heading dates. Isprs J Photogramm. 123, 35–46.
Qiu, B., Huang, Y., Chen, C., Tang, Z., Zou, F., 2018. Mapping spatiotemporal dynamics of maize in China from 2005 to 2017 through designing leaf moisture based indicator from Normalized Multi-band Drought Index. Comput Electron Agr. 153, 82–93.
Qiu, B., Li, H., Tang, Z., Chen, C., Berry, J., 2020a. How cropland losses shaped by unbalanced urbanization process? Land Use Policy. 96, 104715.
Qiu, B., Jiang, F., Chen, C., Tang, Z., Wu, W., Berry, J., 2021. Phenology-pigment based automated peanut mapping using sentinel-2 images. GIScience & Remote Sensing 1–17.
Qiu, B., Hu, X., Chen, C., Tang, Z., Yang, P., Zhu, X., Yan, C., Jian, Z., 2022. Maps of cropping patterns in China during 2015–2021. Sci. Data 9, 479.
Rasul, A., Balzter, H., Ibrahim, G., Hameed, H., Wheeler, J., Adamu, B., Ibrahim, S.a. and Najmaddin, P., 2018. Applying Built-Up and Bare-Soil Indices from Landsat 8 to Cities in Dry Climates. Land. 7.
Rose, S., Kraatz, S., Kellndorfer, J., Cosh, M.H., Torbick, N., Huang, X., Siqueira, P., 2021. Evaluating NISAR's cropland mapping algorithm over the conterminous United States using Sentinel-1 data. Remote Sens Environ. 260, 112472.
Rufin, P., Bey, A., Picoli, M., Meyfroidt, P., 2022. Large-area mapping of active cropland and short-term fallows in smallholder landscapes using PlanetScope data. Int. J. Appl. Earth. Obs. 112, 102937.
Samasse, K., Hanan, N.P., Tappan, G., Diallo, Y., 2018. Assessing Cropland Area in West Africa for Agricultural Yield Analysis. Remote Sensing. 10, 1785.
Shi, T., Li, X., Xin, L., Xu, X., 2018. The spatial distribution of farmland abandonment and its influential factors at the township level: A case study in the mountainous area of China. Land Use Policy. 70, 510–520.
Siebert, S., Portmann, F.T., Döll, P., 2010. Global Patterns of Cropland Use Intensity. Remote Sensing. 2, 1625–1643.
Smith, H., 2019. Evaluating multiple sensors for mapping cropped area of smallholder farms in the eastern Indo-Gangetic Plains.
Tong, X., Brandt, M., Hiernaux, P., Herrmann, S., Rasmussen, L.V., Rasmussen, K., Tian, F., Tagesson, T., Zhang, W., Fensholt, R., 2020. The forgotten land use class: Mapping of fallow fields across the Sahel using Sentinel-2. Remote Sens Environ. 239, 111598.
Waha, K., Dietrich, J.P., Portmann, F.T., Siebert, S., Thornton, P.K., Bondeau, A., Herrero, M., 2020. Multiple cropping systems of the world and the potential for increasing cropping intensity. Global Environ. Change 64, 102131.
Waldner, F., Canto, G.S., Defourny, P., 2015. Automated annual cropland mapping using knowledge-based temporal features. Isprs J Photogramm. 110, 1–13.
Wallace, C.S.A., Thenkabail, P., Rodriguez, J.R., Brown, M.K., 2017. Fallow-land Algorithm based on Neighborhood and Temporal Anomalies (FANTA) to map planted versus fallowed croplands using MODIS data to assist in drought studies leading to water and food security assessments. Mapping Sciences & Remote Sensing. 54, 258–282.
Wang, C., Gao, Q., Wang, X., Yu, M., 2016. Spatially differentiated trends in urbanization, agricultural land abandonment and reclamation, and woodland recovery in Northern China. Sci. Rep. 6, 37658.
Weiss, M., Jacob, F., Duveiller, G., 2020. Remote sensing for agricultural applications: A meta-review. Remote Sens Environ. 236, 111402.
Whelen, T., Siqueira, P., 2018. Coefficient of variation for use in crop area classification across multiple climates. Int. J. Appl. Earth. Obs. 67, 114–122.
Xiong, J., Thenkabail, P.S., Gumma, M.K., Teluguntla, P., Poehnelt, J., Congalton, R.G., Yadav, K., Thau, D., 2017. Automated cropland mapping of continental Africa using Google Earth Engine cloud computing. Isprs J Photogramm. 126, 225–244.
Yin, H., Prishchepov, A.V., Kuemmerle, T., Bleyhl, B., Buchner, J., Radeloff, V.C., 2018. Mapping agricultural land abandonment from spatial and temporal segmentation of Landsat time series. Remote Sens Environ. 210, 12–24.
Zabel, F., Delzeit, R., Schneider, J.M., Seppelt, R., Mauser, W., Václavík, T., 2019. Global impacts of future cropland expansion and intensification on agricultural markets and biodiversity. Nat. Commun. 10, 2844.
Zhu, X., Xiao, G., Zhang, D., Guo, L., 2021. Mapping abandoned farmland in China using time series MODIS NDVI. Sci Total Environ. 755, 142651.